PHYSICAL REVIEW B VOLUME 25, NUMBER 2 15 JANUARY 1982

Self-consistent-average-phonon equation of state. II. Comparison with solid-rare-gas experiments

A. Paskin
Queens College of the City University of New York, Flushing, New York 11367

A. -M. Llois de Kreiner
Brookhaven National Laboratory, Upton, New York 11973

K. Shukla*
Queens College of the City University of New York, Flushing, New York 11367

D. O. Welch and G. J. Dienes
Brookhaven National Laboratory, Upton, New York 11973
(Received 29 June 1981)

The self-consistent-phonon (SCP) formalisms have proved valuable in calculating the anharmonic contributions to lattice-dynamic properties. Replacing the sum over frequencies in the SCP formalism by appropriate functions of the average phonon frequencies yields simple equations of state for solids. This method is called the self-consistent-average-phonon (SCAP) formalism. With the use of empirical Lennard-Jones potentials for neon, argon, krypton, and xenon, the specific heat, lattice parameter, bulk modulus, thermal expansion coefficient, and pressure have been calculated over a range of volumes and temperatures. The SCAP results are compared with the SCP, the improved self-consistent-phonon (ISCP), and experiment for Ar. The ISCP and SCAP are then compared with experiment for Ne, Kr, and Xe. With the use of an empirical Lindemann constant at zero pressure, curves for the pressure along the melting line of solid Ar, Kr, Xe, and Ne are calculated. The agreement between the SCAP results and experiment over a wide temperature range varies from good (better than 10%) to excellent (better than 1%), and establishes the value of using the SCAP formalism to calculate the thermodynamic properties of solids having anharmonic interatomic forces.

I. INTRODUCTION

The self-consistent-phonon (SCP) formalism[1] has proved valuable in calculating the anharmonic contributions to the detailed lattice-dynamic properties of solids (e.g., the phonon dispersion relations). It is, however, a procedure which requires extensive numerical calculations of the characteristic frequencies for a given set of volume and temperature conditions. Calculating properties such as the equation of state and other thermodynamic functions, the results are obtained in numerical form after summing the contribution from each phonon mode. This numerical procedure must be repeated for each new set of conditions.

In calculations of the thermodynamic properties many of the details of the phonon dispersion relations are averaged out in the summation process. This suggests that a self-consistent theory formulated in terms of the average properties might be useful with a considerable reduction in numerical complexity. In this approach, the sums of the various functions of the phonon frequencies are replaced by appropriate average functions of average phonon frequencies. Welch, Dienes, and Paskin[2] have used a classical version of the self-consistent cell model (SCCM) to obtain approximate analytic forms of the equation of state[2,3] for solids. The SCCM has proved to be accurate at high temperatures[3] where the classical model should be valid. With additional (non-self-consistent) quantum modifications, it has been used over the entire temperature range.[2] Because of the success of the quantum-modified SCCM equation of state, it was of interest to investigate the SCP formalism to see if replacing the sums over phonon frequencies by appropriate functions of the average phonon frequency, would also yield accurate

but simple equations of state for solids. We shall refer to this method as the self-consistent-average-phonon (SCAP) formalism. It has the advantage over the SCCM of being a self-consistent quantum calculation and is thus applicable at all temperatures. It has the advantage over the SCP formalism of being simple to use (and analyze) to calculate the thermodynamic properties.

In an earlier paper[4] (I) the equation of state and related thermodynamic equations were developed using the SCAP formalism. The SCAP and SCP results for Ne and Ar were compared[4] at a low and high temperature. A Lennard-Jones potential was used for the interatomic potential for near neighbors and good agreement was found for the L. C. N.-Grüneisen parameter and the bulk modulus at these temperatures. These results encouraged us to test the SCAP formalism against the SCP formalism and against experiment for Ne, Ar, Kr, and Xe over the entire temperature range at zero pressure. Using the Lindemann relationship between the mean-square displacement and the near-neighbor distance at melting, pressure versus melting-temperature curves were generated for Ar, Kr, Ne, and Xe and compared with experiment.

II. SELF-CONSISTENT-AVERAGE-PHONON FORMALISM

In the earlier paper[4] (I), the detailed derivation of the equation of state is presented. Only necessary results are outlined here. The two fundamental self-consistency equations are Eqs. (1) and (2):

$$\langle\omega^2\rangle=\frac{1}{3M}\left\langle\sum_l\nabla^2 v(\vec{R}_{0l}+\vec{u})\right\rangle, \tag{1}$$

where $\langle\omega^2\rangle$ is the average of the square of the frequency, $v(\vec{R}_{0l})$ is the interatomic potential between atoms separated a distance $\vec{R}_{0l}$, the index l denotes atoms neighboring a given origin atom (denoted zero), $\vec{u}=\vec{u}_l-\vec{u}_0$ is the relative displacement of atoms l and 0 from their average equilibrium positions, and M is the atomic mass. The brackets on the right-hand side of Eq. (1) denote a thermal average

$$\langle u^2\rangle=\frac{3\hbar}{M\langle\omega^2\rangle^{1/2}}\coth\xi, \tag{2}$$

where

$$\xi=\tfrac{1}{2}\beta\hbar\langle\omega^2\rangle^{1/2} \text{ and } \beta=(k_BT)^{-1}. \tag{3}$$

In the SCAP formalism, the Helmholtz free energy is given by

$$F=\frac{3}{\beta}\ln(2\sinh\xi)-\frac{3\hbar}{4}\langle\omega^2\rangle^{1/2}\coth\xi+\frac{S_0}{2}+\frac{S_2}{12}\langle u^2\rangle+\frac{S_4}{144}\langle u^2\rangle^2+\frac{S_6}{2592}\langle u^2\rangle^3, \tag{4}$$

where $\xi=\frac{1}{2}\beta\hbar\langle\omega^2\rangle^{1/2}$ and the expression for S_n is listed in the Appendix. The SCAP expressions for pressure, bulk modulus, internal energy, and specific heat are obtained by taking appropriate derivatives of this equation.

The pressure P is obtained by differentiating Eq. (4) with respect to volume at constant temperature:

$$P=-\left.\frac{\partial F}{\partial V}\right|_\beta=-\frac{1}{6V}\left[R_1\frac{dS_0}{dR_1}+\frac{\langle u^2\rangle}{6}R_1\frac{dS_2}{dR_1}+\frac{\langle u^2\rangle^2}{72}R_1\frac{dS_4}{dR_1}\right], \tag{5}$$

where R_1 is the first-neighbor separation; explicit expressions for the lattice-sum derivatives R_1dS_n/dR_1 are listed in the Appendix.

The isothermal bulk modulus B_T is obtained by differentiating the pressure, Eq. (5), with respect to volume:

$$B_T\equiv-V\left.\frac{\partial P}{\partial V}\right|_\beta, \tag{6}$$

or

$$9VB_T=\frac{1}{2}\left[R_1^2\frac{d^2S_0}{dR_1^2}-2R_1\frac{dS_0}{dR_1}\right]+\frac{\langle u^2\rangle}{12}\left[R_1^2\frac{d^2S_2}{dR_1^2}-2R_1\frac{dS_2}{dR_1}\right]+\frac{\langle u^2\rangle^2}{144}\left[R_1^2\frac{d^2S_4}{dR_1^2}-2R_1\frac{dS_4}{dR_1}\right]+\frac{1}{12}R_1\left.\frac{\partial\langle u^2\rangle}{\partial R_1}\right|_\beta\left[R_1\frac{dS_2}{dR_1}+\frac{\langle u^2\rangle}{6}R_1\frac{dS_4}{dR_1}\right], \tag{7}$$

where the lattice-sum derivatives $R_1^2 d^2 S_n / dR_1^2$ are listed in the Appendix. The derivative $R_1 \partial \langle u^2 \rangle / \partial R_1 \mid_\beta$ is essentially of order $\langle u^2 \rangle$ and is obtained from Eqs. (1) and (2) as follows. From Eq. (2) we find

$$R_1 \frac{\partial \langle u^2 \rangle}{\partial R_1}\bigg|_\beta = -A R_1 \frac{\partial \langle \omega^2 \rangle}{\partial R_1}\bigg|_\beta , \tag{8}$$

while differentiating Eq. (1) consistently with Eq. (8) yields

$$R_1 \frac{\partial \langle \omega^2 \rangle}{\partial R_1}\bigg|_\beta = \frac{\frac{1}{3} R_1 \frac{dS_2}{dR_1} + \frac{\langle u^2 \rangle}{18} R_1 \frac{dS_4}{dR_1} + \frac{\langle u^2 \rangle^2}{108} R_1 \frac{dS_6}{dR_1}}{1 + \frac{AS_4}{18M} + \frac{A \langle u^2 \rangle S_6}{108M}} , \tag{9}$$

where A is a function essentially of order $\langle u^2 \rangle$:

$$A \equiv \frac{1}{2\langle \omega^2 \rangle} \left[\langle u^2 \rangle + \frac{3\hbar^2 \beta}{2M} (\coth^2 \xi - 1) \right] , \tag{10}$$

with $\xi \equiv \frac{1}{2} \beta \hbar \langle \omega^2 \rangle^{1/2}$.

An average of the Grüneisen parameter $\gamma_{k\lambda} \equiv -\delta \ln \omega_{k\lambda} / \partial \ln V \mid_\beta$ is immediately obtained by combining Eqs. (1) and (9):

$$\gamma \equiv -\frac{1}{2} \frac{\partial \ln \langle \omega^2 \rangle}{\partial \ln V}\bigg|_\beta = -\frac{1}{6\langle \omega^2 \rangle} R_1 \frac{\partial \langle \omega^2 \rangle}{\partial R_1}\bigg|_\beta$$
$$= -\frac{1}{6} \frac{\left[R_1 \frac{dS_2}{dR_1} + \frac{\langle u^2 \rangle}{6} R_1 \frac{dS_4}{dR_1} + \frac{\langle u^2 \rangle^2}{72} R_1 \frac{dS_6}{dR_1} \right]}{\left[1 + \frac{AS_4}{18M} + \frac{AS_6 \langle u^2 \rangle}{108M} \right] \left[S_2 + \frac{\langle u^2 \rangle}{6} S_4 + \frac{\langle u^2 \rangle^2}{72} S_6 \right]} . \tag{11}$$

This expression was obtained by combining expression for $\langle \omega^2 \rangle$ and $R_1 \partial \langle \omega^2 \rangle / \partial R_1 \mid_\beta$ which are each correct to order $\langle u^2 \rangle^2$ (recognizing that A is essentially of order $\langle u^2 \rangle$).

The internal energy per atom U and the specific-heat capacity at constant volume are obtained by differentiating the free energy with respect to β,

$$U = F + \beta \frac{\partial F}{\partial \beta}\bigg|_V , \tag{12}$$

or, from Eqs. (1) and (4):

$$U = \tfrac{1}{4} M \langle u^2 \rangle \langle \omega^2 \rangle + \frac{S_0}{2} + \frac{S_2}{12} \langle u^2 \rangle + \frac{S_4}{144} \langle u^2 \rangle^2 + \frac{S_6}{2592} \langle u^2 \rangle^3 , \tag{13}$$

where we have retained the term of order $\langle u^2 \rangle^3$ to yield C_V to essentially order $\langle u^2 \rangle^2$. C_V is found by further differentiation:

$$C_V = -\frac{1}{T} \beta \frac{\partial U}{\partial \beta}\bigg|_V$$
$$= -\frac{1}{T} \beta \left[\frac{M}{4} \langle u^2 \rangle \frac{\partial \langle \omega^2 \rangle}{\partial \beta}\bigg|_V + \frac{M}{2} \langle \omega^2 \rangle \frac{\partial \langle u^2 \rangle}{\partial \beta}\bigg|_V \right] . \tag{14}$$

The derivatives of $\langle \omega^2 \rangle$ and $\langle u^2 \rangle$ with respect to β are obtained from Eqs. (1) and (2):

$$\frac{\partial \langle u^2 \rangle}{\partial \beta}\bigg|_V = \left[\frac{\langle u^2 \rangle}{2\langle \omega^2 \rangle} \frac{\partial \langle \omega^2 \rangle}{\partial \beta}\bigg|_V + \frac{3\hbar^2}{2M} (1 - \coth^2 \xi) \left[1 + \frac{\beta}{2\langle \omega^2 \rangle} \frac{\partial \langle \omega^2 \rangle}{\partial \beta}\bigg|_V \right] \right] , \tag{15}$$

and

$$\left.\frac{\partial\langle\omega^2\rangle}{\partial\beta}\right|_V = \frac{\frac{3\hbar^2}{2M^2}\left[\frac{S_4}{18}+\frac{S_6}{108}\langle u^2\rangle\right](1-\coth^2\xi)}{1-\frac{3\hbar}{2M^2\langle\omega^2\rangle^{3/2}}\left[\left[\frac{S_4}{18}+\frac{S_6}{108}\langle u^2\rangle\right][\xi(1-\coth^2\xi)-\coth\xi]\right]}, \tag{16}$$

where $\xi\equiv\frac{1}{2}\langle\omega^2\rangle^{1/2}\hbar\beta$.

Finally, the linear coefficient of thermal expansion at zero pressure α is obtained by recognizing that the zero-pressure near-neighbor distance is obtained by setting the pressure, Eq. (5), to zero and solving for R_1. Thus differentiating Eq. (5) with respect to temperature yields

$$\begin{aligned}\alpha &\equiv \frac{1}{R_1}\frac{dR_1}{dT} \\ &= \frac{1}{6}\frac{\beta}{T}\left.\frac{\partial\langle u^2\rangle}{\partial\beta}\right|_V\left[R_1\frac{dS_2}{dR_1}+\frac{\langle u^2\rangle}{6}R_1\frac{dS_4}{dR_1}+\frac{\langle u^2\rangle^2}{72}R_1\frac{dS_6}{dR_1}\right] \\ &\times\left\{\left\{\left[\left[R_1\frac{dS_0}{dR_1}+R_1^2\frac{d^2S_0}{dR_1^2}\right]+\left[R_1\frac{dS_4}{dR_1}+R_1^2\frac{d^2S_4}{dR_1^2}\right]\frac{\langle u^2\rangle}{6}+\left[R_1\frac{dS_6}{dR_1}+R_1^2\frac{d^2S_6}{dR_1^2}\right]\frac{\langle u^2\rangle^2}{72}\right]\right.\right. \\ &\left.\left.+\frac{R_1}{6}\left.\frac{\partial\langle u^2\rangle}{\partial R_1}\right|_\beta\left[R_1\frac{dS_2}{dR_1}+\frac{\langle u^2\rangle}{6}R_1\frac{dS_4}{dR_1}\right]\right\}\right\}^{-1}\end{aligned} \tag{17}$$

where $\partial\langle u^2\rangle/\partial R_1|_\beta$ and $\partial\langle u^2\rangle/\partial\beta|_V$ are obtained from Eqs. (8), (9), (15), and (16), and $\langle u^2\rangle$, $\langle\omega^2\rangle$, as well as the various lattice coefficients, are evaluated at the appropriate zero-pressure volume.

In numerical calculations, three modifications of the SCAP formalism were used: SCAP(1) in which terms to order $\langle u^2\rangle$ were retained in the self-consistency and thermodynamic equations: SCAP(2) where terms to order $\langle u^2\rangle^2$ were kept in all equations; and SCAP(3) where terms to order $\langle u^2\rangle$ were retained in the self-consistency equations and terms to order $\langle u^2\rangle^2$ in the thermodynamic equations. The "hybrid" treatment was found successful in the SCCM calculations and was found to give the best agreement in the present calculations.

rare-gas solids have been found to be well described by the Lennard-Jones potential, and

III. NUMERICAL RESULTS

In order to compare theory with experiment, an appropriate interatomic potential is needed. The

rare-gas solids have been found to be well described by the Lennard-Jones potential, and
further, this form has been commonly used in theoretical formalisms. Thus, the Lennard-Jones potential may be used to compare formalisms as well as to compare with rare-gas solid data. While there are many other potentials which may be used for more detailed comparisons with rare-gas solids they do not seem justified at this time in the present comparisons. The potential has been used in the form

$$v(R)=\epsilon\left[\left[\frac{R_0}{R}\right]^{12}-2\left[\frac{R_0}{R}\right]^{6}\right], \tag{18}$$

where ϵ and R_0 are parameters to be determined by an empirical fit. The potential was here extended to second neighbors and thus ϵ and R_0 will differ somewhat from either the near-neighbor or infinite-neighbor treatments. R_0 was chosen to match the experimental lattice parameter at $T=0$ K as is commonly done. ϵ was chosen so that the classical energy was equal to the experimental binding energy. This choice of ϵ was found to also

TABLE I. Values of ϵ and R_0 used in the Lennard-Jones potential. The Lindemann parameter $L = \langle u^2 \rangle^{1/2}/R_1$.

	Ne	Ar	Kr	Xe
ϵ (10^{-16} ergs)	67.735	212.007	290.632	409.149
R_0 (Å)	3.0536	3.7410	3.9994	4.3553
L	0.091	0.081	0.081	0.081
a (kbar)	1.2	2.11	2.5	3.0

give a good match to the low-temperature bulk modulus. The use of this ϵ in the SCAP formalisms because of zero-point energy contributions gave energy at $T=0$ K somewhat different from the observed binding energies. Thus ϵ might be thought of as a parameter chosen to match the bulk modulus, although the procedure was more circuitous, as indicated.

It should be noted that in the SCAP(2) and SCAP(3) formalisms, terms to order $\langle u^2 \rangle^2$ were retained in both the numerator and denominator in the various expressions involving $\langle u^2 \rangle$. The thermodynamic properties F, P, B_T, α, C_V, C_P, U, and γ were calculated for the SCAP formalisms on the CDC-7600 computer. An iterative algorithm was used which obtained $\langle u^2 \rangle$ and $\langle \omega^2 \rangle$ self-consistently to one part in 10000 and then inserted into the appropriate thermodynamic equations. A complete set of this data over a wide range of volumes and temperature required several minutes of computing time.

In Table I, a list is given of the empirical parameters used in subsequent calculations. The values of R_0 are chosen to fit the $T=0$ K lattice parameter and the value of ϵ is chosen to fit the classical binding energy at $T=0$ K. In Figs. 1–4,

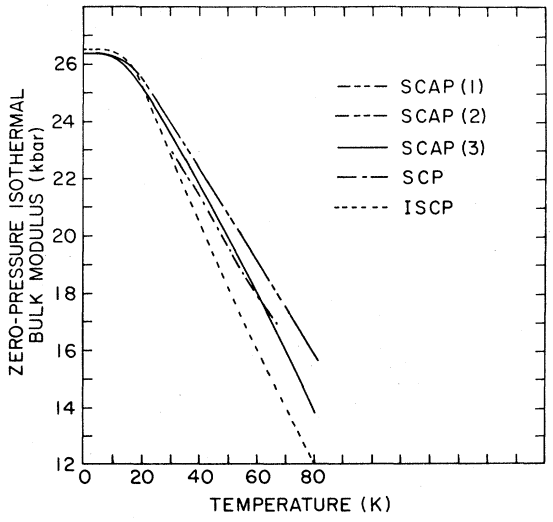

FIG. 1. The zero-pressure isothermal bulk modulus in kbar as a function of temperature for Ar. The SCP, ISCP, SCAP(1), SCAP(2), and SCAP(3) theoretical curves are shown.

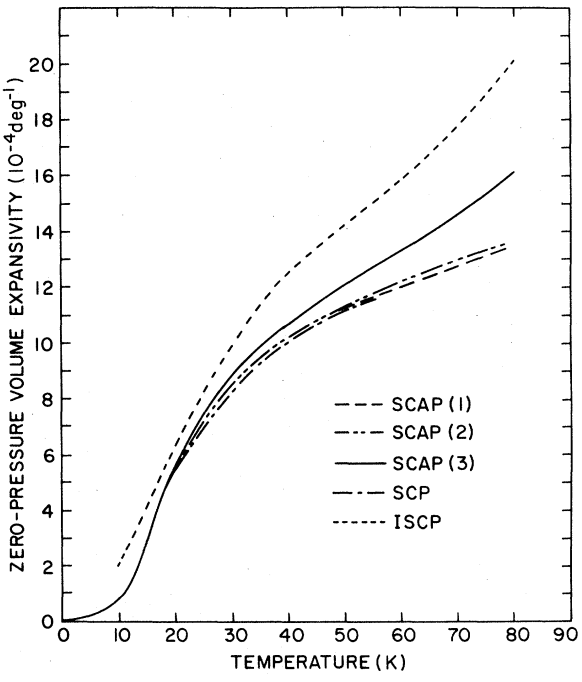

FIG. 2. The zero-pressure volume expansivity in 10^{-4} deg^{-1} as a function of temperature for Ar. The SCP, ISCP, SCAP(1), SCAP(2), and SCAP(3) theoretical curves are shown.

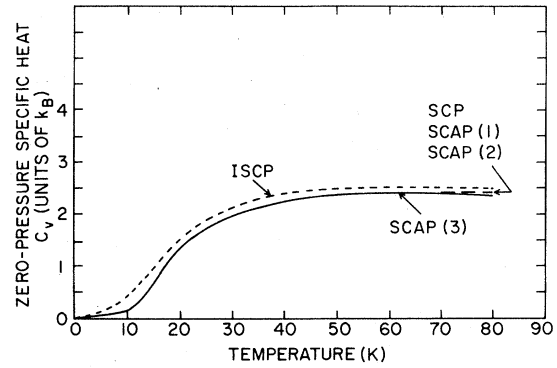

FIG. 3. The zero-pressure specific heat C_V in units of k_B as a function of temperature for Ar. The SCP, ISCP, SCAP(1), SCAP(2), and SCAP(3) theoretical curves are shown.

the various self-consistent formalisms are compared for ^{40}Ar. That is in each treatment, ϵ and R_0 have been chosen to fit Ar, and therefore comparisons between the various formalisms can be made. The SCP (Ref. 5) and ISCP (Refs. 6 and 7) treatments are for interatomic potentials extending to all neighbors, and the various SCAP treatments restrict the interactions to first and second neighbors. While this changes the values of ϵ and R_0, the results are not significantly affected by these differences.

If ISCP, as it will subsequently be seen is the better fit to experiment at the highest temperature, is used as the "standard" curve to be fit by other calculations, it is clear in Figs. 1—3 for Ar that SCAP(3) is the best fit of the SCP and SCAP(1)

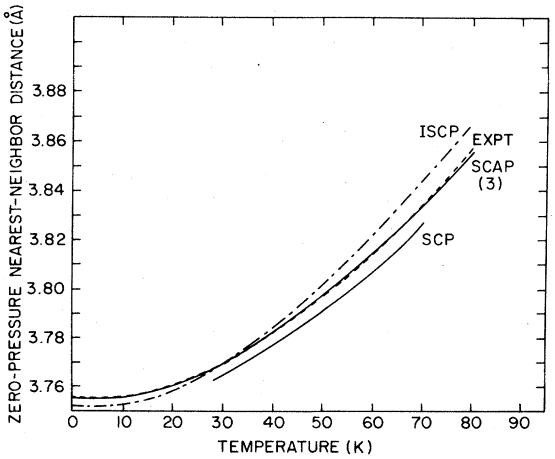

FIG. 4. A comparison of zero-pressure nearest-neighbor-distance data for Ar with theory. The experimental data are from Ref. 8.

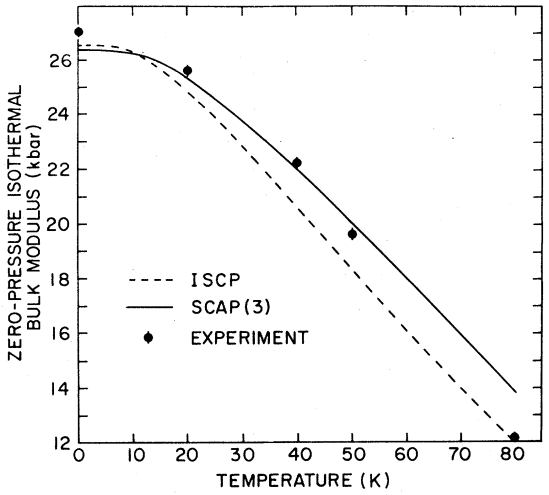

FIG. 5. A comparison of zero-pressure isothermal bulk-modulus data for Ar with theory. The experimental data are from Ref. 8.

and SCAP(2) formalisms. In the subsequent comparisons of theory and experiment, the SCAP(3) and ISCP calculations will mainly be given. It might further be noted that from low to medium temperatures the SCP and SCAP formalisms give about the same results whereas the ISCP deviates from these treatments in the medium-temperature

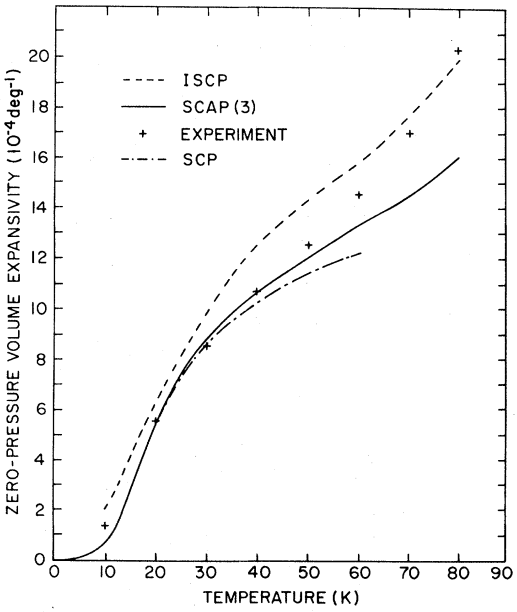

FIG. 6. A comparison of zero-pressure volume-expansivity data for Ar with theory. The experimental data are from Ref. 8.

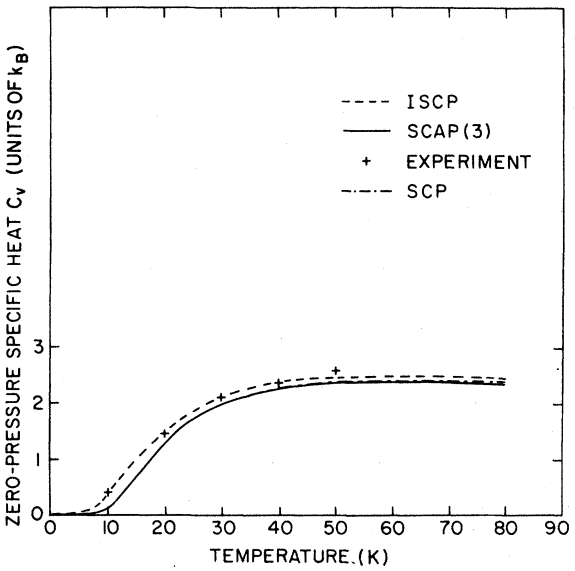

FIG. 7. A comparison of zero-pressure specific heat C_V data for Ar with theory. The experimental data are from Ref. 9.

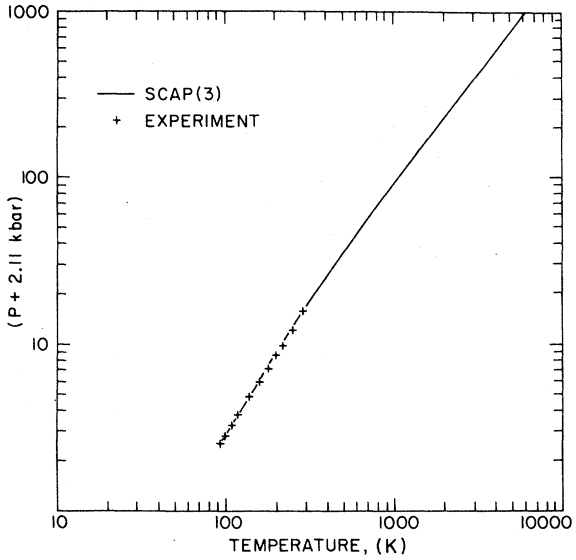

FIG. 9. The pressure along the melting curve for Ar. The pressure plus 2.11 kbar is plotted versus the melting temperature. The experimental data are from Refs. 11 and 12.

range. Thus, the ISCP high-temperature results are obtained at the cost of some low-to-medium temperature adjustments. There are possible complications in the analysis of the high-temperature results arising from vacancy formation. These effects will be discussed in more detail in the discussion of Kr.

In Figs. 4—9 for Ar, the experimental near-neighbor distance is in excellent agreement with SCAP(3) and in notably poor agreement with either ISCP or SCP calculations while the bulk modulus is in agreement with SCAP(3) in the low- and medium-temperature range but about 15% off near the melting point. Conversely, the ISCP is about 10% off in the medium-temperature region

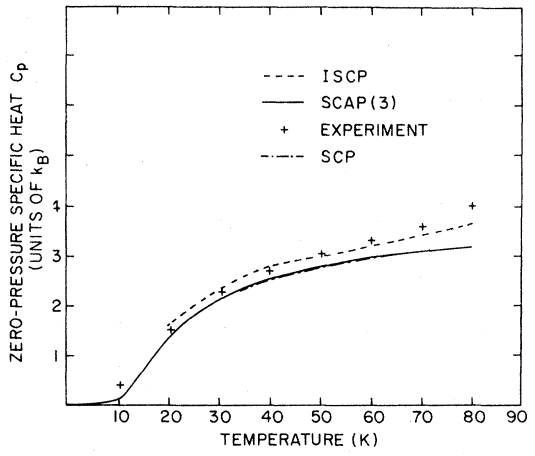

FIG. 8. A comparison of zero-pressure specific heat C_P data for Ar with theory. The experimental data are from Ref. 10.

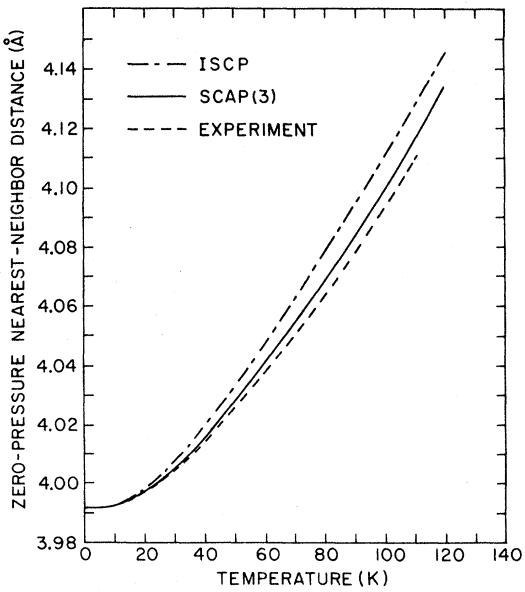

FIG. 10. A comparison of the zero-pressure nearest-neighbor distance for Kr with theory. The experimental data are from Ref. 13.

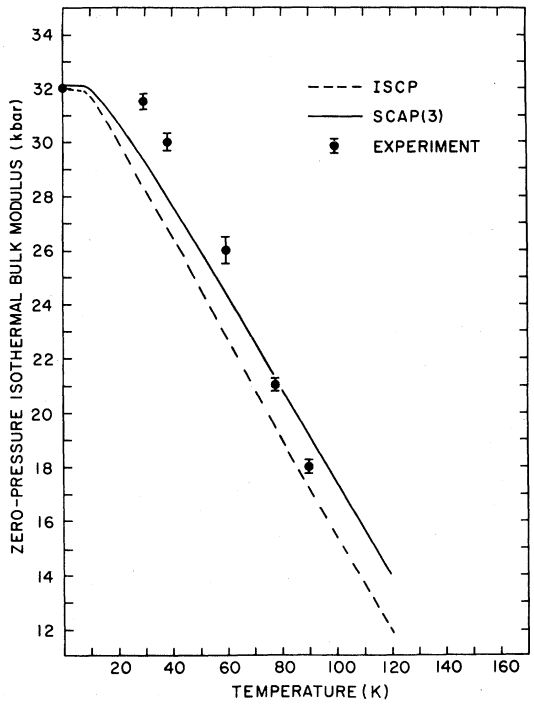

FIG. 11. A comparison of the zero-pressure isothermal bulk modulus for Kr with theory. The experimental data are from Ref. 14.

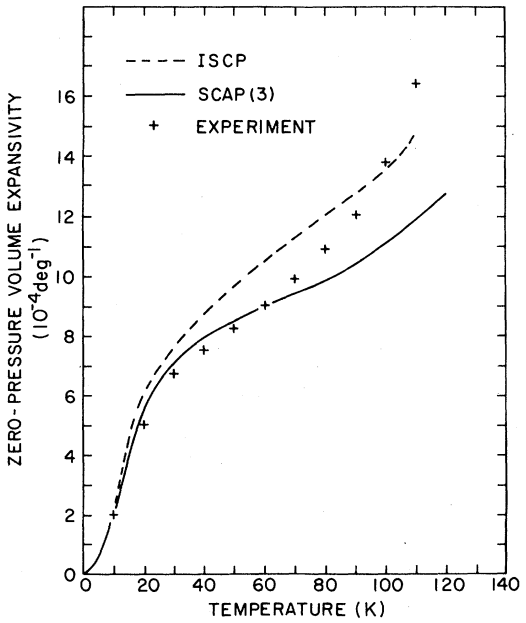

FIG. 12. A comparison of the zero-pressure volume expansivity for Kr with theory. The experimental data are from Ref. 13.

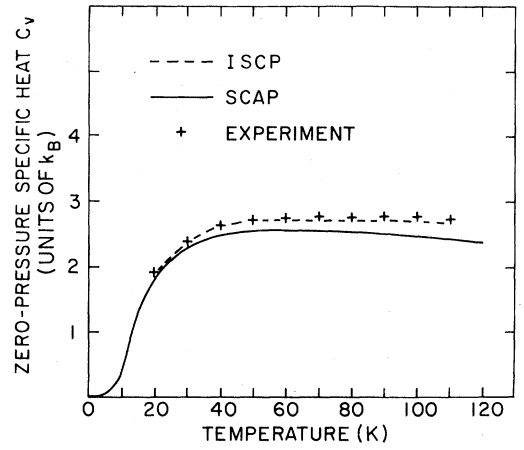

FIG. 13. A comparison of the zero-pressure specific heat C_V for Kr with theory. The experimental data are from Refs. 9 and 13.

but in agreement at the melting point. Similar regimes of applicability occur for the volume expansivity. In the case of the specific heat, the ISCP results are in better agreement with experiment over the entire temperature range. Thus, it is clear that none of the formulations is in better agreement with experiment than the others for all thermal properties over the entire temperature range. It would appear that all of the formalisms examined here are approximations to the true equation of state. Thus, the choice of any formalism must be guided by the temperature range that is desired, as well as the particular property of interest.

Similar comparisons are made for Kr in Figs. 10–15. Again, as seen in Fig. 10, the lattice

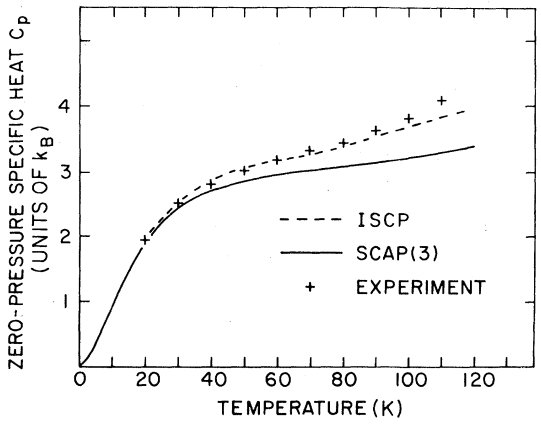

FIG. 14. A comparison of the zero-pressure specific heat C_P for Kr with theory. The experimental data are from Ref. 9.

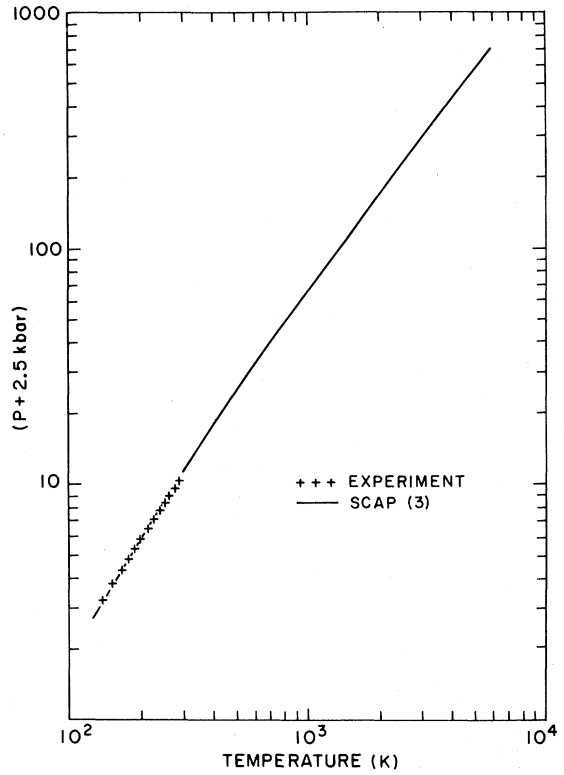

FIG. 15. A comparison of the pressure along the melting curve for Kr with theory. The pressure plus 2.5 kbar is plotted verus the melting temperature. The experimental data are from Ref. 15.

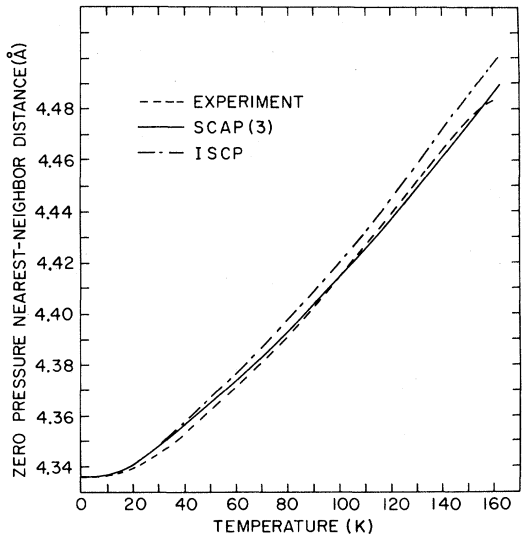

FIG. 16. A comparison of the zero-pressure nearest-neighbor distance for Xe with theory. The experimental data are from Ref. 16.

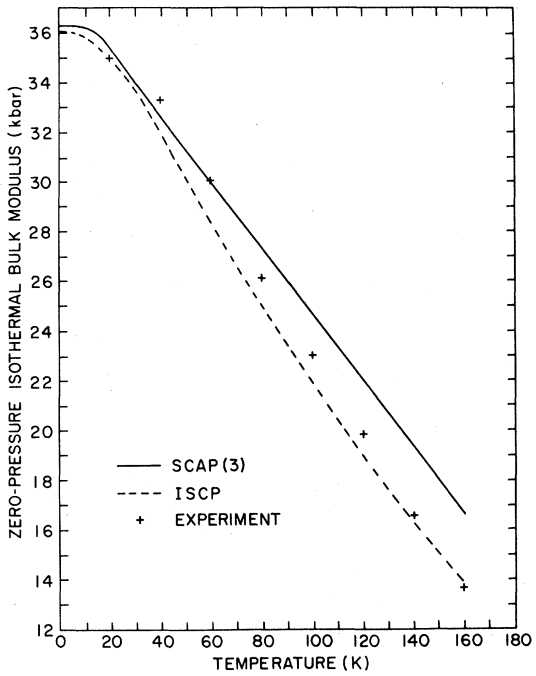

FIG. 17. A comparison of the zero-pressure isothermal bulk modulus for Xe with theory. The experimental data are from Ref. 16.

parameter is better described by the SCAP(3) formalism, whereas for the bulk modulus the ISCP does better in the vicinity of the melting point while SCAP(3) does better at medium temperatures. Similar behavior is found for the volume expansivity. While there are only small differences between SCAP(3) and the ISCP results for C_V, the C_P ISCP results are in better agreement in the medium-to-high temperature regions.

In the region near melting, from 80 to 110 K, a comparison of the volume expansivity obtained by bulk measurements and x-ray lattice-parameter

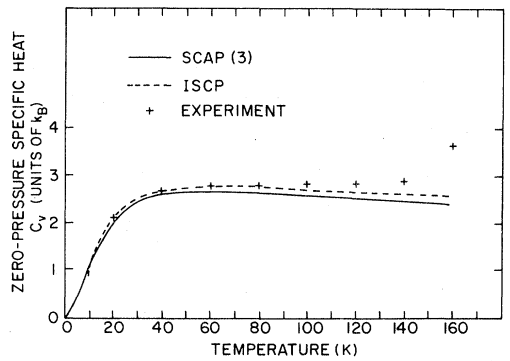

FIG. 18. A comparison of the zero-pressure specific heat C_V for Xe with theory. The experimental data are from Refs. 16 and 17.

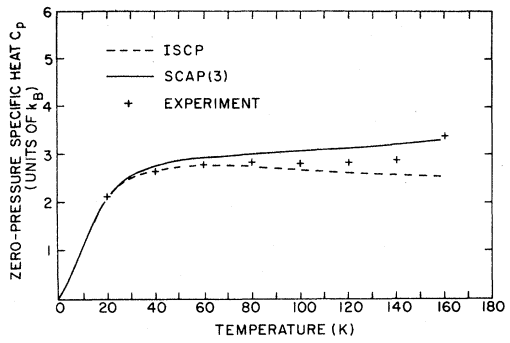

FIG. 19. A comparison of the zero-pressure heat C_P for Xe with theory. The experimental data are from Refs. 16 and 17.

measurements[13] yields direct evidence for vacancy formation. Thus, for Kr (and most likely for all the rare-gas solids by corresponding states arguments),[13] all measurements in the high-temperature regime are on nonperfect lattices with vacancies present. While data such as the expansivity data based on x-ray data of Fig. 12 have the explicit volume effects of vacancies subtracted, it it not obvious how to treat implicit anharmonic effects arising from the vacancies.[13] Thus, the deviations of experiment above 80 K may arise from a failure of the SCAP formalism to treat accurately the anharmonicity of a perfect lattice or it may also arise from the anharmonic contributions arising from the defects and their effects on the lattice modes. As this is outside the scope of the present paper,[13] the deviations of the SCAP from thermodynamic data near the melting point must be treated with some reservations.

The same general characteristics are again observed in Figs. 16–21 for Xe. Neon has been saved for last as it is a rare-gas solid that, in general, has been found to be described more poorly by the self-consistent phonon treatments than the the other (less quantum) rare-gas solids, as seen in Figs. 22–26. Further, as good bulk modulus data do not exist, ϵ is not well defined for the potential used in the SCAP formalism and thus comparison with experiment has more uncertainty. In Fig. 22 the near-neighbor distance is compared with the SCAP results. This is the poorest match to experiment of all of the rare-gas solids. The SCP results are included; clearly they have not been matched to the low-temperature data. If they had been, the results would not differ much from the SCAP results and would likewise not match the rather large change in near-neighbor distance at high temperatures. The bulk modulus data are not very complete and hence comparisons cannot be made over most of the temperature range. The specific-heat calculations of C_V and C_P are in poor agreement with experiment over most of the temperature range while the calculated volume expansivity

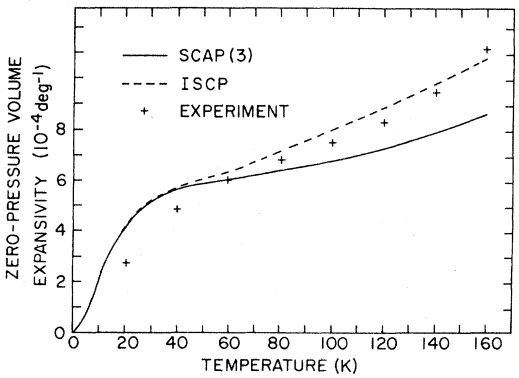

FIG. 20. A comparison of the zero-pressure volume expansivity for Xe with theory. The experimental data are from Ref. 16.

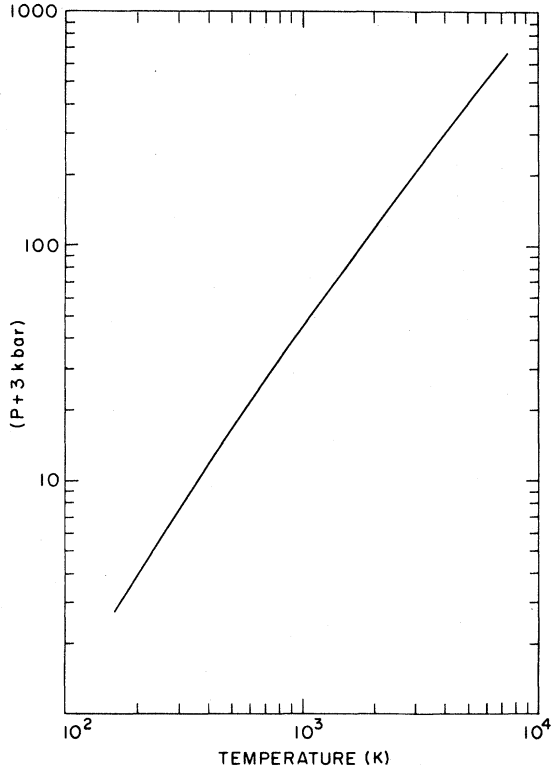

FIG. 21. The pressure along the melting curve for Xe. The pressure plus 3 kbar is plotted versus the melting temperature.

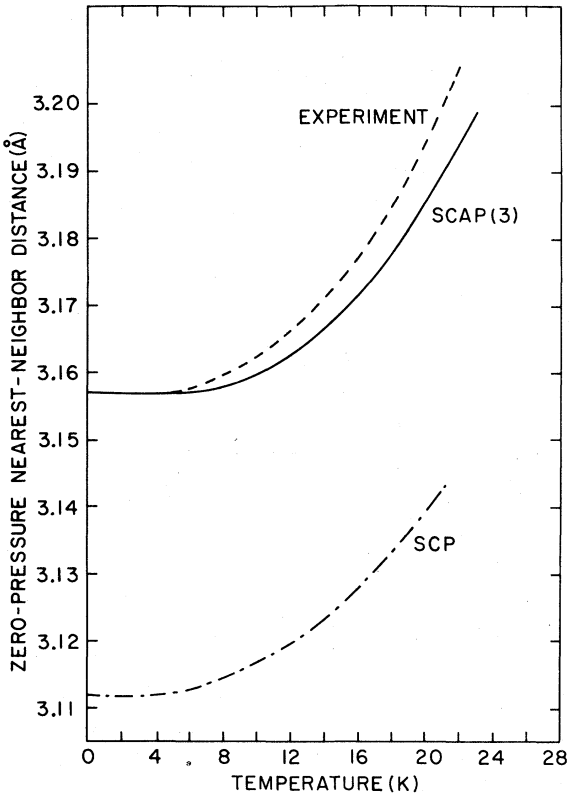

FIG. 22. A comparison of the zero-pressure nearest-neighbor distance for Ne with theory. The experimental data are from Ref. 18.

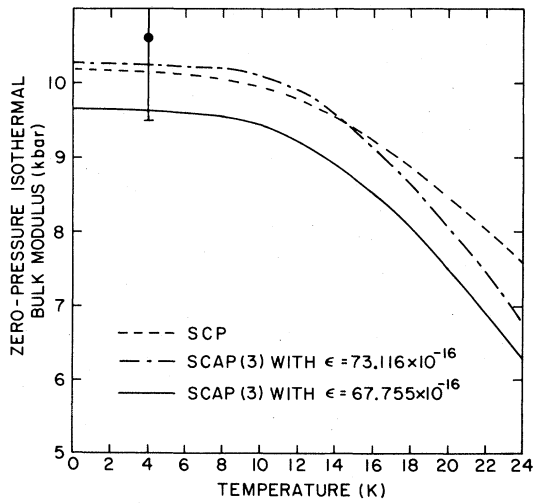

FIG. 23. A comparison of the zero-pressure isothermal bulk modulus for Ne with theory. The experimental data are from Ref. 19.

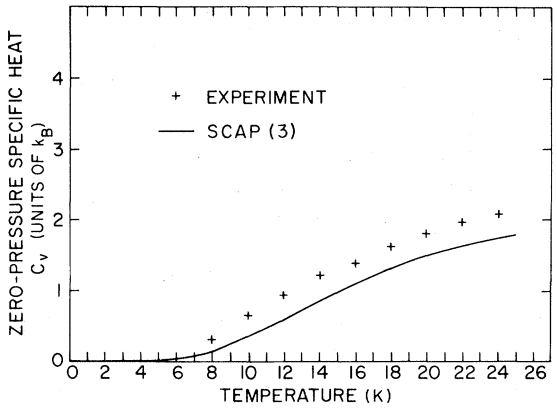

FIG. 24. A comparison of the zero-pressure specific heat C_V for Ne with theory. The experimental data are from Ref. 17.

seems systematically shifted from experiment in a similar way. Clearly Ne is not as accurately described by the self-consistent phonon treatments as are Ar, Kr, and Xe. While this is not surprising, it does indicate that the SCAP treatments do not provide an accurate description of the "very quantum" solids with light masses, such as Ne and He.

The pressure along the melting line is a useful relationship for testing the equation of state. Excellent results were obtained in Figs. 9, 15, and 27 by assuming that the root-mean-square displacement divided by the near-neighbor distance (the Lindemann constant) is a constant, independent of pressure at the melting point. The appropriate value is chosen for each element from the zero-pressure value at the known melting temperature and used for extrapolation to all pressures. It was found that a Lindemann parameter of $L=0.081$ matches all the rare-gas solids (except Ne for

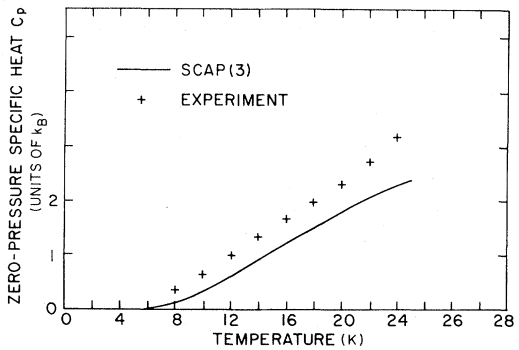

FIG. 25. A comparison of the zero-pressure specific heat C_P for Ne with theory. The experimental data are from Ref. 17.

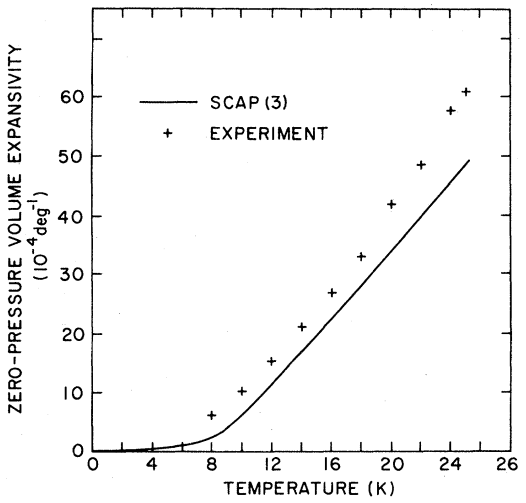

FIG. 26. A comparison of the zero-pressure volume expansivity for Ne with theory. The experimental data are from Ref. 15.

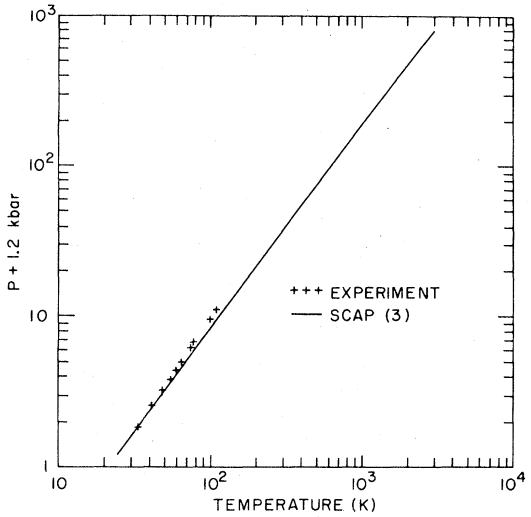

FIG. 27. The pressure along the melting curve for Ne. The pressure plus 1.2 kbar is plotted versus the melting temperature. The experimental data are from Ref. 15.

which $L=0.091$) (Figs. 9 and 15). In the cases of Ar and Kr, the theoretical curve is in excellent agreement with experiment. For Ne, Fig. 27, the agreement is not as good at the highest temperatures, as it is for Ar and Kr. A curve for Xe is also given, even though data do not exist at present. It is also of interest to see how well the Simon equation describes experiment[15] and theory. The Simon equation may be written

$$(P+a)=a(T/T_0)^c\,, \tag{19}$$

where a and c are adjustable parameters and T_0 is the temperature of the triple point. To compare with the Simon equation, our results have been plotted in the form of $(P+a)$ vs T, where a was chosen to have the data give an approximate linear dependence on the melting temperature on a log plot. It can be seen that using the values of a in the table, approximate linearity is observed over the range of pressure data that is now available. At higher pressures deviations from linearity are predicted by the SCAP calculations.

In the case of Kr, an overall better fit is obtained between theory and experiment using $a=2.5$ kbar rather than $a=1.6$, as suggested by Crawford and Daniels. While the choice of a does not affect the high-pressure data, it does shift the low-pressure data considerably. It would be of interest both to extend the pressure range as well as have pressure data taken for Xe. It is always a more convincing demonstration of the power of a theory to make predictions that are subsequently confirmed by experiments. On the basis of the Kr and Ar results, experiment should confirm the theoretical curve in Fig. 21.

IV. CONCLUSIONS

It is apparent that for all but the more quantum-like solids, the self-consistent average phonon formalism is an accurate means of calculating the anharmonic properties of solids in the low-to-medium temperature range. While it is a reasonable approximation even up to the melting point, there is no question that the improved self-consistent phonon approximation is necessary to obtain accurate results in the temperature range near the melting point (with some sacrifice at lower temperatures). If an analytic formalism is desired near the melting temperature, the self-consistent cell model also does an excellent job. The formalisms which one chooses for average thermal properties is at the moment a matter of which temperature range is of interest, as well as which formalism proves convenient to the user. Having worked with the SCAP and SCCM formalisms, we find them easy to apply to new solids. Others familiar with the SCP and ISCP formalisms, having established the computational machinery, may find these simpler to use. The purpose of these calculations was to demonstrate

the relative accuracy of the SCAP formalisms, and this is clearly seen in the extensive curves for the rare-gas solids. It is hoped that this procedure will be further tested for other solids for which pair potentials exist, much as we have applied the self-consistent cell model to copper and iron. The SCCM and SCAP formalisms seem to be particularly useful for obtaining the pressure along the melting curve.

Note added in proof. The recent data of P. R. Granfors, A. T. Macrander, and R. O. Simmons [Phys. Rev. B 24, 4953 (1981)] on crystalline xenon for the compressibility and thermal expansion remove some of the high-temperature discrepancies between SCAP(3) and experiment. The data now lie between ISCP and SCAP(3) at the highest temperatures.

ACKNOWLEDGMENTS

Work done at Brookhaven National Laboratory is supported by the Division of basic Energy Sciences, U.S. Department of Energy, under Contract No. DE-AC02-76CH00016.

APPENDIX: EXPLICIT EXPRESSIONS FOR LATTICE SUMS OF DERIVATIVES OF THE INTERATOMIC POTENTIAL WHICH APPEAR IN THE SCAP EQUATIONS

In the following expressions the sums are over neighbors, labeled l, to a given origin atom. The derivatives of the potential are with respect to its argument and are evaluated at the mean inter-neighbor spacing.

For $n=0,2,4,6$:

$$S_n \equiv \sum_l (\nabla^2)^{n/2} v(R_l) = \sum_l \left[\frac{d^n v}{dR^n} + \frac{n}{R} \frac{d^{(n-1)} v}{dR^{(n-1)}} \right]_l , \tag{A1}$$

$$R_1 \frac{dS_n}{dR_1} = \sum_l \left[R \frac{d^{(n+1)} v}{dR^{(n+1)}} + n \frac{d^n v}{dR^n} - \frac{n}{R} \frac{d^{(n-1)} v}{dR^{(n-1)}} \right]_l , \tag{A2}$$

$$R_1^2 \frac{d^2 S_n}{dR_1^2} = \sum_l \left[R^2 \frac{d^{(n+2)} v}{dR^{(n+2)}} + nR \frac{d^{(n+1)} v}{dR^{(n+1)}} - 2n \frac{d^n v}{dR^n} + \frac{2n}{R} \frac{d^{(n-1)} v}{dR^{(n-1)}} \right]_l . \tag{A3}$$

---

*On leave from the University of Rajasthan, Jaipur 302004, India.

[1]For a review of self-consistent phonon and related formalisms, see H. R. Glyde and M. L. Klein. Crit. Rev. Solid State Sci. 2, 181 (1971).

[2]D. O. Welch, G. J. Dienes, and A. Paskin, J. Phys. Chem. Solids 39, 589 (1978).

[3]G. J. Dienes, D. O. Welch, and A. Paskin, J. Phys. Chem. Solids 41, 1373 (1980).

[4]K. Shukla, A. Paskin, D. O. Welch, and G. J. Dienes, Phys. Rev. B 24, 724 (1981).

[5]N. S. Gillis, N. R. Werthamer, and T. R. Koehler, Phys. Rev. 165, 951 (1968).

[6]M. L. Klein, V. V. Goldman, and G. K. Horton, J. Phys. Chem. Solids 31, 2441 (1970).

[7]V. V. Goldman, G. K. Horton, and M. L. Klein, Phys. Rev. Lett. 21, 1527 (1968); Phys. Lett. 28A, 341 (1968).

[8]O. G. Peterson, D. N. Batchelder, and R. O. Simmons, Phys. Rev. 150, 703 (1966).

[9]R. H. Beaumont, H. Chihara, and J. A. Morrison, Proc. Phys. Soc. London 78, 1462 (1961).

[10]P. Flubacher, A. J. Leadbetter, and J. A. Morrison, Proc. Phys. Soc. London 78, 1449 (1961).

[11]R. K. Crawford and W. B. Daniels, Phys. Rev. Lett. 21, 367 (1968).

[12]V. M. Cheng, W. B. Daniels, and R. K. Crawford, Phys. Lett. 43A, 109 (1973).

[13]D. L. Losee and R. S. Simmons, Phys. Rev. 172, 944 (1968).

[14]A. O. Uras, D. L. Losee, and R. O. Simmons, J. Phys. Chem. Solids 28, 2269 (1967).

[15]R. K. Crawford and W. B. Daniels, J. Chem. Phys. 55, 5651 (1971).

[16]J. U. Trefny and B. Serin, J. Low Temp. Phys. 1, 23 (1969).

[17]H. Fenichel and B. Serin, Phys. Rev. 142, 490 (1966).

[18]D. N. Batchelder, D. L. Losee, and R. O. Simmons, Phys. Rev. 173, 873 (1968).

[19]J. Stewart, Phys. Rev. 97, 578 (1955).